# Molecular Dynamics Simulations of the Resting and Hydrogen Peroxide-Bound States of Cytochrome *c* Peroxidase†

J. R. Collins, P. Du, and G. H. Loew*

*Molecular Research Institute, 845 Page Mill Road, Palo Alto, California 94304*

*Received March 17, 1992; Revised Manuscript Received August 20, 1992*

ABSTRACT: The current hypothesis for the formation of the catalytically active compound I of peroxidases from the resting state and peroxide involves formation of a reversible "inner-sphere" complex in which the peroxide is bound to the heme iron. It is this precursor that is postulated to then form compound I. However, this crucial putative transient intermediate has not yet been definitively detected or characterized by experimental methods. We report here the use of energy minimization and molecular dynamics simulation together with the known X-ray structure of cytochrome *c* peroxidase to investigate the nature of this complex and comparisons of it with the resting state in which a water is bound as a ligand. Among the properties monitored in these simulations are the mode of binding of the peroxide to the heme iron, its interactions with neighboring amino acid residues, and the extent to which the binding of the peroxide perturbs both the local environment around the heme unit and more distant regions. The results of this study indicate that solvated, full protein dynamics is required to obtain reliable results for the known resting-state complex and hence for the uncharacterized peroxide complex. In this complex, the peroxide binds to the heme iron in a dynamically averaged end-on fashion, rather than a bridged structure, with approximately equal probability of each oxygen serving as the ligand to the iron. Binding of the peroxide as a ligand disrupts the H-bonded network of waters in the distal binding pocket which are present in the resting state, but there is no dramatic perturbation of the nearby amino acid residues. The peroxide hydrogen forms a stable H-bond with the Nε of His52, and the peroxide oxygen is quite near the HNε of Arg48. These results provide additional evidence for the postulated role of these two residues in the O–O bond scission of the peroxide complex to form compound I. On the proximal side, a stable H-bond is found between the carboxyl oxygens of the nearby Asp235 and both the proximal His ligand and the Trp191 residue that is stacked over it, providing further evidence that the imidazole is deprotonated. In addition to an "inner-sphere" peroxide complex, very preliminary indication is found for the formation of an "outer-sphere" precursor complex, in which the peroxide is bound near a highly conserved residue, Pro145 in the distal pocket, but not as a ligand of the heme iron.

Peroxidases are heme enzymes that utilize hydrogen peroxide, alkyl hydroperoxides, or peroxo acids to perform two sequential oxidations of substrates. The ferric resting state of these enzymes is converted to the catalytically active state by a catalytic cycle that has been shown to be the same for all hydroperoxidases (Frew & Jones, 1984). It involves (i) binding of the peroxide and (ii) formation of a twice-oxidized active intermediate, a ferryl-oxo, compound I state. Oxidations by compound I proceed through a once-reduced compound II intermediate to the ferric resting state.

Although peroxidases share a common mechanism for formation of compound I, they can be differentiated by the types of oxidations they perform. One of the most extensively studied peroxidases, horseradish peroxidase (HRP) (Dunford & Stillman, 1976), is typical of one type that binds substrates near the heme unit with oxidation occurring by chemical transformation, usually involving sequential H abstractions. By contrast, two other well-studied peroxidases, cytochrome *c* peroxidase (CCP) (Yonetani & Ray, 1965; Yonetani, 1965) and lignin peroxidase (LIP) (Tien, 1987; Gold et al., 1989), are typical of the other type that oxidize surface-bound substrates by long-range electron transfer. LIP catalyzes the oxidation of surface-bound polycyclic aromatic hydrocarbons and anisole analogues, in addition to its natural phenylpropanoid polymeric substrate, lignin. The natural substrate for CCP is another protein, cytochrome *c*. CCP differs from the other peroxidases in that its initial compound I state quickly forms a variation called compound ES, in which the heme unit abstracts an electron from a nearby amino acid (Yonetani, 1970), now thought to be Trp191 on the proximal side of the heme (Sivaraja et al., 1989).

The part of the catalytic cycle common to all hydroperoxidases, the mechanism of formation of compound I, has been the subject of intense experimental interest over the past two decades. These studies have largely focused on HRP and, to a lesser extent, CCP. Many of the most recent investigations on CCP have been concerned with the identity of the nearby amino acid that is oxidized to form compound ES (Goodin et al., 1987; Mauro et al., 1988; Sivaraja et al., 1989). While there are many unresolved aspects in the formation of compound I by the peroxidases, detailed kinetic studies (Jones & Dunford, 1977; Baek & Van Wart, 1989) of HRP and CCP have led to a number of very useful insights and provide guidelines and constraints for the formulation of a mechanism consistent with the observations.

A seminal observation is that, while the rate constant for compound I formation from the resting state is 3 orders of magnitude lower than that expected for a simple diffusion-controlled bimolecular reaction, the activation energy is less than that for a diffusion-controlled reaction (Jones & Dunford, 1977; Baek & Van Wart, 1989). The most conservative

† We thank the National Science Foundation for financial support of this work (Grant DMB-9096181) and the Pittsburgh Supercomputer Center and NCI supercomputer center at Frederick, MD, for supercomputer support.

* Author to whom correspondence should be addressed.

0006-2960/92/0431-11166$03.00/0 

mechanism of compound I formation consistent with these apparently disparate observations is that at least one reversible precursor complex is formed, prior to compound I formation, i.e.

$$E + H_2O_2 \rightleftharpoons \text{precursor complex} \rightarrow \text{compound I} \quad (1)$$

and that the observed rate constant for compound I formation is

$$k_{obs} = K_p k_{ox} \quad (2)$$

where $K_p$ is the equilibrium constant for formation of the reversible precursor complex ($K_p = k_1/k_{1'}$) and $k_{ox}$ is the rate of formation of compound I from the precursor complex (Jones & Dunford, 1977).

The precursor complex is thought to be an "inner-sphere" complex in which the peroxide binds to the heme iron, in keeping with the general model of inner-sphere redox reactions. Experimental evidence for this type of mechanism is that the first-order saturation kinetics, predicted from it, have been verified experimentally (Baek & Van Wart, 1989). Additional evidence, observation of a transient electronic spectrum involving an oxidized enzyme–peroxide complex labeled compound 0 in HRP, has also been cited (Baek & Van Wart, 1989).

While the proposed involvement of a reversible precursor inner-sphere complex in compound I formation is consistent with observed kinetic behavior, it still leaves many unanswered questions. Chief among these is the detailed mechanism of both steps in pathway 1: (i) formation of the inner-sphere complex and (ii) formation of compound I from it. Water has been found as a ligand in the resting state of the only known peroxidase structure CCP (Finzel et al., 1984), suggesting that the formation of an inner-sphere precursor complex must occur by a substitution reaction in which the peroxide takes the place of the water ligand. Such a substitution can in principle proceed by one of two types of mechanism (Swaddle, 1974): (i) an "associative mechanism" involving a seven-membered transition state, in which the water and peroxide are simultaneously bound to the iron leading directly to the inner-sphere complex, and (ii) a dissociative mechanism in which the water ligand leaves first, forming a five-coordinated intermediate that binds the peroxide. The possibility of a direct substitution reaction proceeding by a dissociative mechanism is difficult to envision since the upper limit for a dissociative mechanism is determined by the rate of release of the leaving ligand. In the associative mechanism, it is also difficult to understand how HOOH displaces $H_2O$ as the sixth ligand, since molecular HOOH is a poor nucleophile and is not expected to be competitive with water as the sixth ligand. One possibility is that HOOH could destabilize the hydrogen-bond network around the ligand water, making the water more mobile and thus more amenable to either direct displacement or the formation of the seven-membered transition structure, leading to an associative mechanism of substitution. Another possibility is that the peroxide acquires at least partial anionic character in the binding site of the protein and acts more like a peroxy anion, an excellent nucleophile, that could easily displace water to form the inner-sphere complex.

The experimental constraints on the participation of $HO_2^-$ in the substitution reaction leading to the inner-sphere complex are, however, considerable (Jones & Dunford, 1977). First, kinetic studies have shown that pathways involving pre-equilibrium formation of the anion complex are not consistent with experiment. Second, the peroxidases CCP and HRP do not bind anions such as $F^-$, $CN^-$, and peroxo anions. Thus, if $HO_2^-$ is the species that interacts with the heme iron, it appears that it must be formed inside the binding pocket. In addition, the proton released must remain inside the protein and be balanced by a proton uptake in compound I formation to be consistent with the absence of a pH effect on the reaction rate and the observation that a proton is neither released nor taken up in compound I formation (Jones & Dunford, 1977; Davies et al., 1976).

Taken together, the known experimental constraints on the reaction mechanism point to the following steps for the formation of compound I: (i) An "outer-sphere" complex is formed, in which the peroxide binds in the distal heme pocket but not as a ligand of the heme iron. Argument in favor of this complex is the possibility that it could disrupt the H-bond network around the ligand water and allow HOOH to acquire at least partial anionic character, making it more competitive for replacing the water ligand. (ii) An associative substitution reaction of the ligand water in the resting state of the enzyme by HOOH takes place, leading to a reversible inner-sphere complex. (iii) Rapid formation by the inner-sphere complex of compound I by O–O bond scission and the net formation of water occur.

While these steps constitute a plausible and consistent mechanism, it is not a proven one. For example, it invokes transient states of the enzymes that have not yet been observed and are very difficult to observe and characterize by experimental methods alone. With the solution of the crystal structure of CCP (Finzel et al., 1984), computational simulations can now be used to further probe some structural and dynamic aspects of the proposed mechanism.

In the work reported here, we have performed empirical energy minimization and molecular dynamics (MD) simulations of the resting state and the inner-sphere peroxide complex of CCP. The purpose of this work is threefold. Since this is the first study to focus on the ligand interactions and the dynamic behavior of this enzyme, we wish, by use of the known properties of the resting state, to determine the level of approximation appropriate for reliable molecular dynamics simulations for the uncharacterized transient inner-sphere complex.

Second, by characterization of the dynamic behavior of the resting state and the transient complex we wish to obtain insight into the nature and mechanism of formation of the inner-sphere complex. On the basis of the crystal structure of CCP, it was suggested that in the precursor complex the peroxide displaces the water ligand bound to iron, as well as two additional waters, labeled 596 and 648 (Finzel et al., 1984), with the peroxide located between the positions previously occupied by waters 596 and 648 in this complex. The results presented here were used to examine the plausibility of this hypothesis.

Third, by examining the minimized structures and dynamic behavior of the inner-sphere complex, we wish to characterize key interactions with nearby residues and bound waters on the distal and proximal sides of the heme unit implicated in the formation of compound I (Poulos & Finzel, 1984). Chief among these in the distal peroxide pocket are His52 and Arg48. His52 is thought to act as a proton-transfer agent, first accepting a proton from the oxygen bound to the iron forming the peroxoanion and then donating it to the other oxygen to form $H_2O$ as the O–O bond breaks. The proposed role for the positively charged species, Arg48, is to promote charge separation in the transition state. On the proximal side, interactions of the ligand His175, Arg235, and Trp191

Table I: Parameters[a] for the $H_2O$ and Peroxide Ligand and for Fe Used in the Simulatinos of the CCP Resting and Peroxide-Bound States

| Bonding Parameters for HOOH[b] | | | | |
|---|---|---|---|---|
| | | force constant | equilibrium value | degeneracy |
| bond distance | H–O | 553.0 kcal/Å$^2$ | 0.950 Å | |
| bond distance | O–O | 535.0 kcal/Å$^2$ | 1.475 Å | |
| bond angle | H–O–O | 35.0 kcal/deg$^2$ | 94.8° | |
| torsion angle | H–O–O–H | 4.0 kcal/deg$^2$ | 180.0°[c] | 3.0 |

| van der Waals Parameters | | |
|---|---|---|
| | A | B |
| O | 141.8 | 9.285 |
| H | 0.02 | 0.04 |
| Fe | 0.1081 | 0.2940 |

| Partial Charges (in Units of Electrons) | | | |
|---|---|---|---|
| H (peroxide) | 0.312 | Fe | 1.25 |
| O (peroxide) | –0.312 | H (water) | 0.343 |
| | | O (water) | –0.686 |

[a] The parameters were derived to match experimental values where possible. [b] Parameters for hydrogen peroxide [based on data from Figuere (1950)]. [c] This value is the phase parameter in the torsional potential.

have also been monitored since they have been proposed to be important for facile compound I formation and intramolecular electron transfer to the heme unit.

## METHODS

Molecular mechanics optimizations and molecular dynamics simulations of the peroxide-bound and resting states of CCP have been performed using the program AMBER (3.0) (Weiner & Kollman, 1981) and the united atom force field, with explicit consideration of polar hydrogen atoms (Weiner et al., 1984). The use of the united atom approach for protein dynamics simulations has been established as a reliable approximation in a number of calculations (Wampler et al., 1990; Daggett & Kollman, 1990; Ferguson et al., 1991). Parameters for the hydrogen peroxide molecule, including charges on the O and H atoms, are given in Table I, as well as the charges used for the water ligand. The parameters for the heme unit including the atomic charges were taken from the imidazole-ligated heme unit distributed with AMBER. However, nonbonded parameters were modified for the Fe atom to give agreement with the known Fe–$H_2O$ geometry in a model ferric–diaquo–protoporphyrin IX complex (Scheidt et al., 1979). The charge on Fe was increased to +1.25, in close agreement with INDO calculations on Fe(III) porphyrins, and the van der Waals parameters for Fe, given in Table I, were determined by adjusting the radius and well depth of Fe to reproduce the model crystal structure when the diaquo model was minimized. These modifications were necessary since the parameters distributed with AMBER (3.0) did not yield even qualitatively correct structures for the water ligands with the model heme when the water molecules were not explicity bonded to the iron.

The crystal structure of the resting state of CCP, including the crystallographic waters (Finzel et al., 1984), was energy minimized using 200 steps of steepest descent followed by the conjugate gradient method until the RMS gradient fell below 0.1 kcal/Å. A distance-dependent dielectric of $\epsilon = 4R$ and a residue-based nonbonded cutoff of 10 Å were used. This structure served as the starting point for molecular dynamics simulations for the approximation called model 1.

In a second approximation, model 2, full protein molecular dynamics simulations were performed. The initial structure for this simulation was generated by adding a 9 Å solvent shell of water molecules around the minimized protein using the BLOB option of AMBER and reorienting the water molecules in the electric field of the system. The solvated protein, including the 2718 noncrystal solvent molecules, was energy minimized with the same protocol used for model 1 but with a dielectric of $\epsilon = 1$.

In docking the HOOH as a ligand for the heme iron, one OH group of the peroxide was placed in the corresponding oxygen and hydrogen positions of the ligand water in the optimized resting state. The second oxygen of the peroxide was placed at the gas-phase O–O equilibrium distance (1.475 Å) from the ligand oxygen and the second H position at the OH bond length of peroxide and its equilibrium torsion angle of 122°. This initial geometry corresponds to an "end-on" peroxide complex. No other bound waters were removed from the structure. The hydrogen positions of all the crystallographic water molecules were allowed to relax during a 1-ps MD simulation at 100 K, with the oxygen positions constrained by a positional force constant of 0.1 kcal/Å$^2$. As for the resting state, two models for the peroxide-bound state, one with just the crystallographic waters (model 1) and the second with the added solvation shell (model 2), were energy minimized prior to the MD simulations.

MD simulations were performed in two approximations: one called model 1 and the other called model 2, for both the resting and HOOH-bound states of CCP. Detailed analysis of the computational aspects effects of these approximations have been discussed previously (Collins & Loew, 1992) In model 1, where only the crystallographic waters were included, a distance-dependent dielectric constant ($\epsilon = 4R$) was used to mimic an aqueous environment, and the "belly" option of AMBER was used to freeze all residues and crystallographic waters in the protein except those within approximately 15 Å of the heme iron (Brown & Kollman, 1987). Those residues allowed to move freely in model 1 are listed in Table II. The MD simulations were run for 30 ps at a constant temperature of 300 K and a coupling constant of 0.4 ps. The first 5 ps was discarded as a heating and equilibration period before properties were calculated. As shown in a previous study with this model, the total energy remains constant during the last 25 ps, providing evidence for equilibration. The nonbonded pair list was updated every 25 steps, and a 1-fs integration time step was used. Coordinate sets were saved every 0.1 ps.

In model 2, which included the 2718 noncrystal solvent waters, a residue-based cutoff of 9 Å was employed and full protein MD simulations were performed with a constant dielectric of 1.0 for the electrostatic terms. For these simulations, the time step was reduced to 0.5 fs and the nonbonded pair list was updated every 50 steps. The temperature was maintained at 300 K by weakly coupling the system to a heat bath using a constant of 0.5 ps. Coordinate sets were saved every 0.2 ps. The heating was performed in four stages prior to equilibration and simulation. First, using a 300 K initial velocity distribution, all atoms were constrained with a harmonic force constant of 10 kcal/Å$^2$ for 1 ps. Second, using the final velocities of step 1 as input and reducing the harmonic force constant to 5 kcal/Å$^2$, the run was continued for another 1 ps. In step 3, the simulations were continued for another 2 ps with a reduced harmonic force constant of 1.0 kcal/Å$^2$. Finally, in step 4, the harmonic force constant was reduced to 0.5 kcal/Å$^2$ and the trajectory continued for 2 ps. This heating procedure was identical for the resting and the peroxide-bound states. Using the resulting configuration and velocity obtained from the four initial heating steps,

Table II: Amino Acid Residues and Bound Water Molecules Allowed to Move Freely in Constrained Molecular Dynamics Simulations of CCP Resting State and CCP–HOOH Complexes[a]

Y36

Y42, G43, P44, V45, L46, V47, R48, L49, A50, W51, H52, T53, S54, G55, T56, W57

Y71

D79, P80, S81, N82, A83, G84, L85, Q86, N87, G88

G142, R143, L144, P145, D146, A147, D148, K149

Y153, V154

F157, F158, Q159, R160, L161

V168, V169, A170, L171, M172, G173, A174, H175, A176, L177, G178, K179, T180, H181, L182, K183, Q184, S185, G186, Y187, E188, G189, P190, W191, G192

F202

Y229, M230, M231, L232, P233, T234, D235, Y236, S237, L238

waters
345, 348, 376, 379, 382, 384, 408, 441, 443, 444, 445, 446, 447, 477, 535, 596, 648, 653, 742, 743, 745, 746, 747, 784, 785, 895, 896

[a] Residues listed by their number in X-ray structure and one letter code. The residues are separated into regions of contiguous backbone sequences. The water molecules allowed to move freely are listed at the end.

Table III: Effect of Optimized Peroxide Geometry and Energy by Binding to Heme Iron of CCP

| | in vacuo | in CCP |
|---|---|---|
| < OOH bond angle (deg) | 96.2 | 92.8 |
| $\tau$ HOOH (deg) | 121.5 | 1.4 |
| $E_{HOOH}$ (kcal/mol) | 6.9 | 10.2 |

Table IV: Optimized Ligand–CCP Interaction Energies

| ligand | r (Fe–O) (Å) | $E_{VDW}$ | $E_{electrostatic}$ | $E_{H\text{-}bond}$ | $E_{total}$[a] |
|---|---|---|---|---|---|
| $H_2O$[b] | 2.04 | 2.3 | −31.9 | −0.6 | −30.2 |
| HOOH | 2.12 | 4.7 | −25.6 | | −20.9 |

[a] $E_{total} = E_{VDW} + E_{electrostatic} + E_{H\text{-}bond}$. [b] $E_{H_2O}$ = 0.5 kcal/mol.

equilibration was achieved in 20 ps as evidenced by the asymptotic behavior of the total energy (Collins & Loew, 1992). Full protein simulations require a longer time to achieve equilibration because there are more long-distance interactions which are not optimally described by the finite cutoff distance (9 Å) of nonbonding interactions. The subsequent 20-ps simulations were used to collect data for analysis. To prevent the 2718 solvent molecules from "boiling" away from the protein, the oxygen atoms were constrained using a positional force constant of 0.5 kcal/Å$^2$, while the rest of the protein, including the crystallographically determined waters, was allowed to move freely. The purpose of this constraint is to inhibit the translational motions of the outer water molecules and thus mimic the influences of bulk solvent. A full periodic boundary calculation would be necessary if we were focusing on the dynamic properties of the protein surface. Since all of the properties of interest in this work are centered around the active site, the approximation of a small constraint on the oxygen atom of the solvent waters should be adequate.

Among the properties monitored were the molecular dynamic averaged position and the mean square deviation from this average for every atom in the protein. Crystallographic thermal parameters ($B$ factors) were also calculated by multiplying the mean square deviations by $8\pi^2$ (Brooks et al., 1987). In addition, the instantaneous difference between the Fe–O distances for the two HOOH oxygen atoms was also monitored during the simulation.

## RESULTS

Table III gives the optimized geometries and energies of peroxide in vacuo and bound to the heme iron in CCP. Table IV gives the energy of the ligand–protein interaction for the optimized resting and peroxide-bound complexes for model 2. Also given in this table is the decomposition of the interaction energy into electrostatic, van der Waals, and H-bonding contributions. Figure 1 depicts the active site for the optimized model 2 complexes. Included in these figures are the heme unit and key residues and bound waters on both the distal and proximal sides of the heme. Especially important on the distal side are the ligand, the three residues His52, Trp51, and Arg48, implicated as putative catalytic residues in compound I formation; Pro145 and Ser81; a network of H-bonded waters that interact with the ligand (waters 596, 445, 648, and 747); and a few additional waters H-bonded to the Arg48 (waters 348 and 784). Highlighted on the proximal side are the ligand His175 residue and nearby residues Asp235 and Trp191 and water 535, H-bonded to Asp235. Proton donation from the His175 imidazole to Asp235 has been postulated to be an important part of peroxidase function, while Trp191 is the residue that has been implicated in electron donation to the heme unit in compound I.

The comparisons of the computed $B$ factors for the protein C$\alpha$ atoms derived from the 20-ps trajectories (model 2) with those derived from crystallographic data for the resting state are shown in Figure 2. The interatomic distances calculated from the minimized structures, and the MD average distances, computed over the course of each trajectory, for the same key residues and water molecules in the active site shown in Figure 1, are listed in Table V. The computed mean square deviations from its average position for specified atoms in each of these residues and of the oxygen atoms of the bound waters are given in Table VI. Figure 3 shows a multiple-time exposure of two of the waters involved in the H-bonded network with the ligand water taken every 1 ps from the model 2 MD simulation of the resting state, illustrating the movement of these water molecules in the heme binding pocket. Figure 4 shows a multiple-time exposure, taken at 1-ps intervals for the 25-ps simulation with model 1, for the HOOH molecule bound in the distal pocket but not as a ligand of the heme iron, a putative "outer-sphere complex". Figure 5 shows a plot of the difference between the peroxide ligand O1–Fe and O2–Fe distances during the MD simulation of the model 2 peroxide–

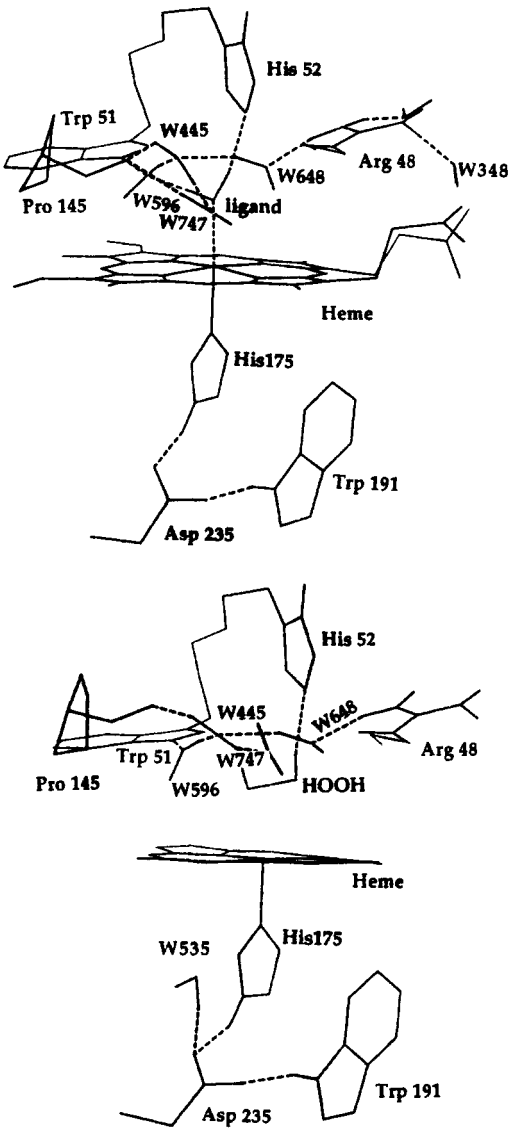


FIGURE 1: Hydrogen-bonding networks for (A, top) the resting state and (B, bottom) the HOOH-bound complex of CCP are shown for the active site including the heme unit, bound $H_2O_2$, and residues His52, Trp51, and Arg48 on the distal side and residues His175, Asp235, and Trp191 on the proximal side. The structures are taken from the minimized geometry of model 2.

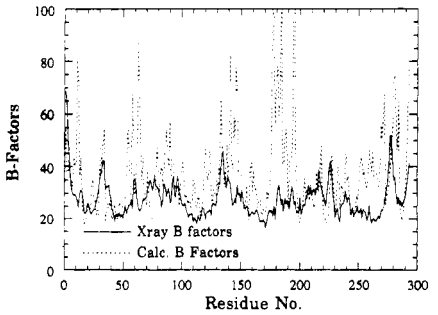


FIGURE 2: Crystallographic and computed *B* factors plotted vs residue number for the Cα atoms of CCP. The mean square deviation taken from the last 20-ps simulation with model 2 has been multiplied by $8\pi^2$ to obtain the computed values.

CCP complex. In the figure, a value of 0.0 indicates that the two oxygen atoms are equidistant from the Fe atom.

## DISCUSSION

As shown in Table III, in the optimized CCP–HOOH complex, peroxide binds to the heme iron in an end-on fashion with a cis configuration, compared to the lowest energy gas-phase form in which the internal torsion angle for the peroxide is 121.5°. The peroxide in the protein assumes a less favorable configuration because of unfavorable steric interactions of the lowest energy form with the porphyrin ring atoms. As shown in Table IV, the optimized Fe–O distance in the peroxide-bound complex is only 0.1 Å greater than that found for the optimized Fe–$OH_2$ distance. In the optimized water-ligated complex, the water ligand forms a much more stable complex with the ferric heme of CCP than the peroxide-bound complex. As shown in Table IV, this difference is largely electrostatic in origin since the net charge on the oxygen atom in peroxide (–0.312) is about half that on the oxygen of the water molecule (–0.686) (Table I). However, if the water is kept at its longer distance of 2.4 Å found in the X-ray structure, its interaction with the protein is significantly reduced to –19.2 kcal/mol. Taking into account differences in the internal energy of the ligands themselves (0.5 for $H_2O$; 10.2 for HOOH), the water still forms a much more stable complex. Such a difference in stability clearly illustrates the challenge of explaining how peroxide rapidly substitutes for the water ligand. To help understand this process, we monitored various aspects of the dynamic behavior of each complex.

Analysis of the minimized resting state of CCP with model 2 (Figure 1A), shown in Table V, indicates that the water molecules in the heme binding pocket form a quite stable hydrogen-bond network with four other bound waters, as suggested by the crystal structure. Each of these water molecules forms multiple H-bonds, with each other and with His52, Trp51, and Arg48. In the optimized CCP–HOOH complex with model 2 (Figure 1B), the pattern of H-bonding and the geometries of the protein and bound water molecules remain essentially the same, although the hydrogen-bond network is not as interconnected in the peroxide complex.

While the minimized resting-state and peroxide-bound complexes give similar active site geometries, the dynamic behavior of each is quite different. The results obtained illustrate two important points. First, the approximations used in performing the simulations can have a dramatic effect on the results, necessitating comparison with experiment for validation before inferences can be made. Second, optimized substrate–protein structures alone generally provide little insight into the perturbations caused by different ligands binding to the heme iron on the bound waters and nearby residues in the distal binding pocket.

The results in Tables V and VI reveal that in the constrained MD simulations (model 1) the water molecules, including the ligand water, leave the distal binding cavity during the course of the MD trajectory of the resting state of CCP. The average distances of the hydrogen bonds from the MD simulation of model 1 of the resting state of CCP (Table V) as well as the *B* factors computed from the MD trajectory (Table V) both indicate that all of the bound waters on the distal side leave the protein. Only water 535, bound to Asp235 on the proximal side, remains in its original crystal position in this model. This behavior is partly due to the motion of Trp51 and His52. These residues are quite mobile and tend to "sweep" the binding site during the course of the trajectory and give the water molecules a translational energy that pushes them out of the heme binding pocket via the peroxide access channel.

In the unconstrained MD simulation of the solvated protein (model 2), by contrast, the ligand water and the waters in the H-bond network remain in the distal binding pocket of the CCP resting state, results much more consistent with experimental results. To assess the overall motion of the protein,

Table V: Calculated Interatomic Distances[f] for Ligands, Bound $H_2O$, and Key Catalytic Residues in Distal Binding Pocket and Proximal Side of Heme

| | resting state | | | | peroxide bound | | | |
|---|---|---|---|---|---|---|---|---|
| | model 1 | | model 2 | | model 1 | | model 2 | |
| intermolecular pair[a] | min[b] | MD av[c] (SD) | min[b] | MD av[c] (SD) | min[b] | MD av[c] (SD) | min[b] | MD av[c] (SD) |
| (a) Ligand $H_2O$ Interactions | | | | | | | | |
| WatLigO–HemFe | 2.28 | 45.8 (33.1) | 2.04 | 2.1 (0.1) | | | | |
| WatLigO–Trp51HNe | 2.71 | 44.6 (33.2) | 2.88 | 3.3 (0.5) | | | | |
| WatLigO–Arg48HNe | 2.81 | 43.8 (33.6) | 3.22 | 4.6 (0.9) | | | | |
| WatLigH2–His52Ne | 2.21 | 43.6 (33.6) | 1.91 | 2.7 (0.5) | | | | |
| WatLigH1–Wat596O | 2.10 | 40.9 (37.7) | 1.71 | 3.1 (0.5) | | | | |
| (b) Peroxide Ligand Interactions | | | | | | | | |
| PerO1–HemFe | | | | | 2.75 | 7.8 (3.7) | 2.12 | 2.5 (0.2) |
| PerO2–HemFe | | | | | 2.74 | 8.1 (3.5) | 2.53 | 2.6 (0.2) |
| PerH1–His52Ne | | | | | 2.40 | 6.2 (3.1) | 3.00 (108°)[d] | 2.9 (0.7) |
| PerH2–His52Ne | | | | | 2.32 | 6.1 (3.1) | 2.00 (133°)[e] | 2.5 (0.3) |
| PerO1–His52Ne | | | | | 2.98 | 5.9 (3.4) | 3.43 | 3.5 (0.5) |
| PerO2–His52Ne | | | | | 3.11 | 5.9 (3.3) | 2.74 | 3.2 (0.2) |
| PerO1–Trp51HNe | | | | | 3.18 | 6.8 (3.8) | 2.57 | 3.2 (0.7) |
| PerO2–Trp51HNe | | | | | 3.60 | 7.1 (3.6) | 3.76 | 3.3 (0.7) |
| PerH1–Wat596O | | | | | 2.64 | 33.8 (32.2) | 2.11 | 7.1 (2.1) |
| PerO1–Arg48NH2 | | | | | 5.15 | 6.5 (3.1) | 5.56 | 5.9 (0.5) |
| PerO2–Arg48NH2 | | | | | 5.57 | 6.5 (3.1) | 4.51 | 5.3 (0.5) |
| PerO1–Arg48HNe | | | | | 3.17 | 6.5 (3.5) | 3.72 | 4.1 (0.6) |
| PerO2–Arg48HNe | | | | | 3.23 | 6.5 (3.4) | 2.42 | 3.5 (0.4) |
| PerO1–Ser81HOg | | | | | 7.73 | 5.7 (1.0) | 9.12 | 8.0 (0.7) |
| PerO2–Ser81HOg | | | | | 8.88 | 5.4 (1.0) | 9.23 | 8.1 (0.6) |
| PerO1–Pro145O | | | | | 6.09 | 4.5 (1.7) | 7.19 | 7.2 (1.1) |
| PerO2–Pro145O | | | | | 7.50 | 4.4 (1.7) | 7.87 | 7.7 (0.8) |
| (c) Common Distal Binding Pocket Interactions | | | | | | | | |
| Wat596H–Wat445O | 2.09 | 51.9 (29.3) | 1.69 | 2.6 (0.7) | 2.06 | 32.9 (21.4) | 1.80 | 10.1 (0.9) |
| Wat596O–Trp51HNe | 2.04 | 4.4 (2.6) | 1.82 | 2.1 (0.3) | 2.05 | 38.1 (33.5) | 1.92 | 8.4 (3.5) |
| Wat445O–Wat648H | 2.14 | 71.2 (36.6) | 1.86 | 7.3 (3.3) | 2.43 | 41.4 (21.4) | 1.91 | 10.4 (1.3) |
| Wat445H–Wat747O | 2.12 | 251.1 (78.8) | 1.71 | 4.6 (1.0) | 2.04 | 31.7 (18.0) | 1.83 | 10.3 (2.2) |
| Wat648O–Arg48HN2 | 1.98 | 87.7 (99.5) | 1.72 | 6.9 (2.2) | 2.03 | 29.0 (25.0) | 1.80 | 3.2 (0.7) |
| Trp51Ne–HemFe | 4.20 | 3.9 (0.3) | 4.46 | 4.9 (0.4) | 4.56 | 3.8 (0.5) | 4.57 | 4.9 (0.4) |
| His52Ne–HemFe | 5.14 | 5.2 (0.4) | 4.78 | 5.2 (0.3) | 5.41 | 5.0 (0.4) | 5.21 | 5.6 (0.3) |
| Trp51Ne–His52Ne | 4.03 | 3.8 (0.4) | 4.22 | 4.2 (0.3) | 4.95 | 3.6 (0.5) | 4.47 | 4.1 (0.5) |
| His52Ne–Arg48NH2 | 3.75 | 4.0 (0.03) | 3.76 | 4.7 (0.5) | 3.75 | 3.8 (0.4) | 3.61 | 4.2 (0.4) |
| His52Ne–Arg48Cz | 3.73 | 3.9 (0.3) | 3.74 | 4.5 (0.5) | 3.67 | 3.8 (0.3) | 3.60 | 4.1 (0.3) |
| Arg48NH2–HemFe | 6.65 | 7.0 (0.5) | 6.42 | 7.0 (0.4) | 7.04 | 6.8 (0.3) | 6.50 | 7.3 (0.4) |
| Arg48HNe–His52Ne | | | 1.93 | 2.7 (0.6) | | | 2.08 | 2.2 (0.3) |
| Trp51HNe–HemFe | | | 4.08 | 4.4 (0.6) | | | 4.74 | 4.4 (0.6) |
| Arg48Ne–HemFe | | | 5.17 | 6.0 (0.6) | | | 5.39 | 5.9 (0.4) |
| Trp51HNe–His52Ne | | | 3.86 | 3.9 (0.4) | | | 4.19 | 3.8 (0.6) |
| (d) Proximal Residue Interactions | | | | | | | | |
| Asp235Od1–His175HNd | 1.89 | 2.0 (0.2) | 1.72 | 1.8 (0.1) | 1.89 | 2.1 (0.2) | 1.72 | 1.8 (0.1) |
| Asp235Od2–Trp191HNe | 1.85 | 2.1 (0.2) | 1.72 | 1.8 (0.1) | 1.85 | 2.0 (0.2) | 1.72 | 1.8 (0.1) |
| Asp235Od1–Wat535H | 2.07 | 3.0 (0.7) | 1.84 | 2.7 (0.3) | 2.33 | 2.9 (0.6) | 1.84 | 2.7 (0.5) |
| His175Nd–Trp191Ne | 3.45 | 3.6 (0.3) | 3.62 | 3.6 (0.3) | 3.41 | 3.5 (0.3) | 3.59 | 3.8 (0.3) |

[a] Each residue is labeled by residue type, number in X-ray structure, and atom for which distance is given. Waters are labeled by number in X-ray structures, WatLig = ligand $H_2O$; Per = peroxide ligand. [b] Calculated distances for minimized structures. [c] MD average distances and standard deviations from MD trajectories. [d] Angle PerO1–PerH$_1$–HisNe. [e] Angle PerO2–PerH$_2$–HisNe. [f] All distances in angstroms.

we have plotted the computed *B* factors for the C$\alpha$ atoms of the protein for this short trajectory and compared them with those derived from the crystal structure. As seen in Figure 2, the overall trends compare reasonably well. Even though this property is quite slow to converge and some of the motion near loops and turns is exaggerated, the overall similarity provides structural criteria for equilibration to complement the asymptotic energy profile during the same simulation interval. Thus, the major inferences for both the resting state and the HOOH complex should be made from the results of this model (model 2), as opposed to model 1.

MD simulations using model 2 for the resting state of CCP were monitored to probe the stability of the H-bond network. From the results listed in Tables V and VI, we see that the distal water ligand is hydrogen bonded to water 596 and His52 and is slightly over 2.5 Å from either Trp51 or Arg48. Three H-bonds are formed by water 596, one to the ligand, one to Wat445, and one to Trp51, providing a bridging H-bond between Trp51 and the ligand. Three H-bonds are also formed by water 445 in the optimized complex, one to each of three waters 596, 648, and 747. Hydrogen bonds are formed between water 747 and waters 445 and 648.

In general, while some portions of the hydrogen-bond network are quite stable in model 2 of the resting state, others show significant dynamic motion and H-bond lengthening. Specifically, in the distal pocket, only waters 596 and 445 and the ligand water remain fairly close to their original positions, as shown in Figure 3, a multiple-time exposure of these three waters in the heme binding pocket. However, during this trajectory, the other two water molecules involved in the H-bonded network with the ligand, Wat648 and Wat784, have high mean square deviations from their average position, indicating that these water molecules are dynamically active and could leave the heme binding site, consistent with their

Table VI: Mean Square Deviation (Å²)[a] from the MD Average Position of Key Atoms in the Active Site for Each of the MD Simulations of the Resting State and Peroxide-Bound State of CCP

| | model 1 | | model 2 | | |
|---|---|---|---|---|---|
| atom | resting state | HOOH | resting state | HOOH | occupancy[b] |
| Arg48Ne | 0.22 | 0.15 | 0.63 | 0.34 | |
| Arg48HNe | 0.40 | 0.23 | 1.0 | 0.40 | |
| Arg48Cz | 0.26 | 0.16 | 0.40 | 0.28 | |
| Arg48NH1 | 0.42 | 0.25 | 0.40 | 0.31 | |
| Arg48NH2 | 0.46 | 0.24 | 0.47 | 0.32 | |
| Trp51Ne1 | 0.30 | 1.00 | 0.48 | 1.5 | |
| His52Ne | 0.30 | 0.31 | 0.45 | 0.36 | |
| Trp191Ne | 0.18 | 0.11 | 0.32 | 0.33 | |
| Asp235Od1 | 0.00 | 0.14 | 0.31 | 0.33 | |
| Asp235Od2 | 0.30 | 0.14 | 0.36 | 0.33 | |
| Wat348O | 4.34 | 10.88 | 2.5 | 1.3 | 1.0 |
| Wat445O | 1018 | 15.99 | 1.6 | 2.1 | 0.91 |
| Wat535O | 1.18 | 0.83 | 0.60 | 0.58 | 1.0 |
| Wat596O | 9.41 | 1216 | 0.71 | 12.1 | 1.0 |
| Wat648O | 2268 | 711 | 17.7 | 1.1 | 0.75 |
| Wat747O | >9999 | 602 | 1.0 | 12.4 | 0.52 |
| Wat784O | 1423 | 1067 | 17.2 | 18.9 | 0.67 |
| Wat/PerLigO | 1215 | 19.58 | 0.44 | 1.1 | |

[a] *B* factors = $8\pi^2 \times$ MSD (mean square deviation). [b] The final colum lists the crystallographic occupancy number for the water molecules for comparison with the X-ray computed numbers.

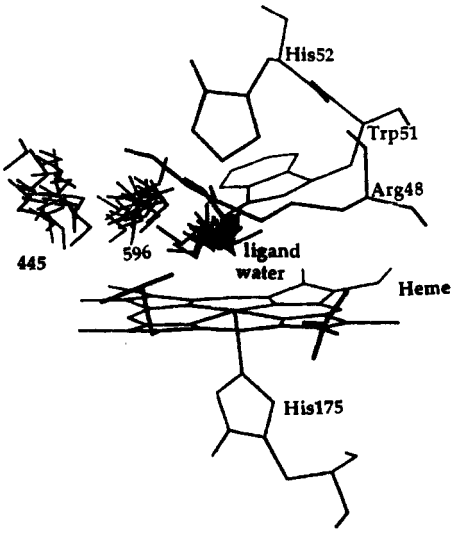


FIGURE 3: Multiple-time exposure of the dynamically stable ligand and distal waters 445 and 596 taken every 1 ps, from the last 20-ps MD simulation of model 2 of the resting state of CCP. This figure illustrates the relative movement of these $H_2O$ molecules in the heme binding pocket.

lower occupancy number in the crystal structure (Table VI). Of the two waters that interact with Arg48, Wat348 and Wat784, Wat348 is stable while Wat784 leaves its original crystal position and moves to a position where it interacts with the bulk waters. These results offer further evidence that bound waters in the distal binding site are mobile and transient and could allow easy access of HOOH into the heme pocket, as required by the kinetic studies. Of particular interest are water molecules 596 and 648, which have been suggested to be replaced by the peroxide when it initially binds (Finzel et al., 1984). Water 596 is fairly stable and may be difficult for HOOH to displace, while water 648 is one of the several more mobile waters that could provide a channel for the HOOH molecule.

In contrast to the resting state in which the ligand $H_2O$ leaves the binding site in constrained MD simulations (model 1), in the HOOH complex, the HOOH ligand does not leave

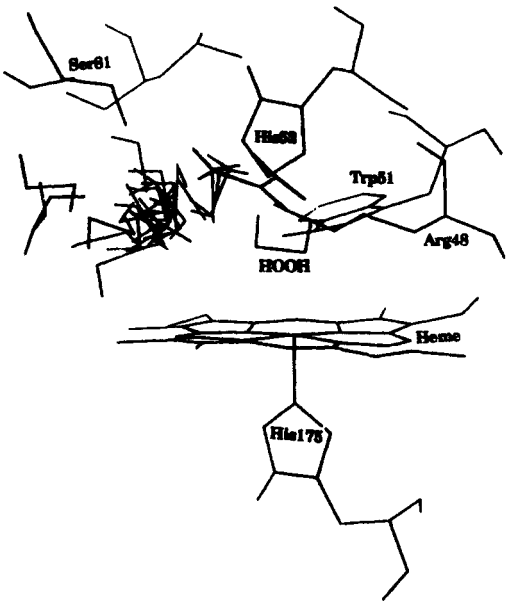


FIGURE 4: Superposition of the optimized HOOH-bound CCP complex with the dynamic motion of the peroxide ligand indicated by a multiple-time exposure (MTF). The MTF is taken from the 25-ps simulation of model 1 for the HOOH-bound CCP complex. In this model, the peroxide does not remain as a ligand but, as indicated, does stay in the distal binding pocket, an indication that an outer-sphere complex can be formed.

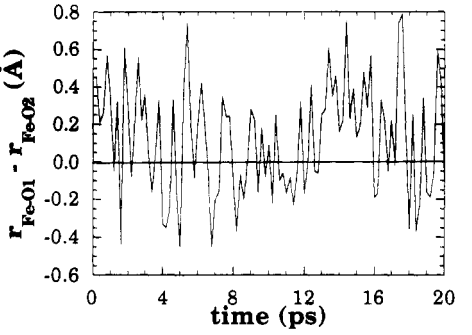


FIGURE 5: Plot of the difference between the $O_1$–Fe and $O_2$–Fe distances for the two oxygen atoms of HOOH during the last 20-ps MD simulation of model 2 of the HOOH-bound state of CCP. A value of 0.0 indicates that the two oxygen atoms are equidistant from the Fe atom and would correspond to a bridged structure. The oscillating (+) and (–) values shown in the figure indicate a rapidly alternating end-on peroxide binding mode.

the binding site. Figure 4 is a multiple-time exposure taken from the 25-ps model 1 MD simulation that shows the position and dynamic behavior of the peroxide in this outer-sphere complex. As shown in Figure 4, the HOOH molecule moves away from the Fe in this model and spends most of its time in the positions previously occupied by water 596 and water 445 in the crystal structure, which have left the binding pocket in this simulation. In this position, the HOOH molecule interacts with the side-chain hydroxyl group of Ser81 and the backbone carbonyl of Pro145 to form a quite stable complex. The differential behavior of the two ligands in this model, the water leaving and the peroxide remaining in the distal pocket, is quite surprising. Despite the limitations of the model, these results do suggest that an outer-sphere complex position of the peroxide may indeed be formed with the peroxide accommodated in the distal binding pocket but not as a ligand to the heme iron.

Since this potentially significant result was obtained using a model with questionable approximations, it should be further tested by both theoretical and experimental studies. Theo-

retically, the question of the existence and optimum form of such an outer-sphere complex should be further investigated by simulation studies using the more reliable model 2 with systematic selection of initial geometries for its formation. If the calculations confirm this outer-sphere complex, it can be tested further experimentally by mutating Pro145 to a residue that would not accommodate peroxide and determining the effect on function. It is interesting to note that Pro145 is conserved in the peroxidases CCP, HRP, turnip peroxidase, and lignin peroxidase (Welinder, 1985; Du et al., 1992). Continued function of the mutant would be evidence against the importance of formation of this outer-sphere complex, while negative results would imply, but not prove, that such a complex may be important.

As shown in Table V, in unconstrained MD simulations (model 2) of the peroxide complex, the H-bonded network of water molecules is totally disrupted and none of the four waters (waters 596, 445, 648, and 747) originally involved in the H-bonding network with the ligand water remain H-bonded to the peroxide or to each other. Water 648 and water 348 both interact with Arg48 and, as shown in Table VI, remain near their equilibrium positions. As also shown in this table, waters 596, 747, and 784 are extremely mobile. Finally, water 445 moves to a position in which it breaks its three H-bonds to waters 596, 648, and 747 (Table IV) but is stable in this new position.

Of major significance is that the unconstrained MD simulations of the peroxide complex (model 2) indicate that this inner-sphere complex formed is dynamically stable, with the peroxide molecule remaining bound to the Fe throughout the simulation. The MD average values of the two Fe–O1 and Fe–O2 distances are nearly equal and suggest a bridged structure. However, a more detailed analysis of the MD simulation (Figure 5) reveals that the peroxide molecule binds in an end-on fashion but with rapidly exchanging oxygen atoms bound to the heme, suggesting the possibility of a low barrier to this exchange with the bridged structure a transition state between the two structures. This behavior is illustrated in Figure 5, in which the difference between the two Fe–O distances is plotted during the course of the trajectory. This difference more accurately displayed the actual dynamics of the HOOH molecule than the averaged values. Flipping between end-on structures results in nonzero values of this parameter, while a value near zero suggests a bridged orientation with respect to the iron. The oscillations between positive and negative values shown in the figures clearly indicate that the HOOH molecule is exchanging oxygen atoms bound to the heme iron, momentarily flipping through a bridged structure. The motion of the HOOH molecule is dominated by the interactions with the iron, HN$\epsilon$ of Trp51, N$\epsilon$ of His52, and HN$\epsilon$ of Arg48, keeping the HOOH in a position to form compound I. This motion also results in an interconversion of the peroxide hydrogen that participates in the H-bond to His52 and of the peroxide oxygen that interacts with Arg48.

This analysis of the MD simulation of the HOOH-bound state of CCP, based on model 2, provides certain insights into the possible interactions involved in the cleavage of the O–O bond, leading to compound I formation. As shown in Tables V and VI, the H-bond between the peroxide molecule and His52 and its proximity to Arg48 are stable. The stability of the interactions of the peroxide ligand with the N$\epsilon$ of His52 and the proximity of Arg48 provides direct evidence supporting the postulated role of each (Poulos & Finzel, 1984) in the formation of compound I from this inner-sphere peroxide complex. In this hypothetical mechanism, His52 is proposed to act as a proton-transfer agent, first accepting a proton from the oxygen bound to the iron to form the peroxo anion and then donating it to the other oxygen to form $H_2O$, leading to the O–O bond breaking. The oscillations of the peroxide also provide additional support for the plausibility of this mechanism. As the peroxide molecule alternates oxygen atoms as the Fe ligand, a proton can be easily taken off one peroxide oxygen and transferred to the other. The role proposed for the positively charged species, Arg48, is to promote facile leaving of the OH group by charge separation in the transition state. The close proximities found between the peroxide hydrogen and the N$\epsilon$ of His52 and between the peroxide oxygen and the HN$\epsilon$ of Arg48 are consistent with these postulated roles.

## CONCLUSIONS

We have investigated how the dynamic interactions of water and peroxide in the heme binding site of CCP may relate to the formation of compound I. Specifically, we have demonstrated that an inner-sphere complex is stable and have examined some of its detailed dynamic properties that may be important to the overall mechanism of compound I formation. The results of these calculations support the previously proposed roles of His52 and Arg48 in the mechanism of O–O bond cleavage of HOOH to form compound I in CCP. Further verification can be obtained by quantum mechanical calculations of the mechanism of O–O bond cleavage that include the effect of the protein. The calculations also suggest that the dynamic role of water in the binding pocket may be more important than previously assumed. In addition, studies using a more approximate model suggest the possible existence of an outer-sphere complex that may precede the formation of the inner-sphere complex. Future studies are planned to address this question of how the formation of an outer-sphere complex may affect the dynamic stability of the H-bond network found in the resting state of CCP.

## ACKNOWLEDGMENT

We thank Dr. Frank Axe for his help in developing the Fe parameter used.

## REFERENCES

Baek, H. K., & Van Wart, H. E. (1989) *Biochemistry 28*, 5714–5719.

Brooks, C. W., III, Karplus, M., & Pettitt, M. (1987) *Adv. Chem. Phys. 71*.

Brown, F., & Kollman, P. A. (1987) *J. Mol. Biol. 198*, 533.

Collins, J. R., & Loew, G. H. (1992) *Int. J. Quantum Chem.: Quantum Biol. Symp.* (in press).

Daggett, V., & Kollman, P. A. (1990) *Protein Eng. 3*, 677–690.

Davies, D. M., Jones, P., & Mantle, D. (1975) *Biochem. J. 157*, 247.

Du, P., Collins, J. R., & Loew, G. H. (1992) *Protein Eng.* (in press).

Dunford, H. B., & Stillman, J. S. (1976) *Coord. Chem. Rev. 19*, 187–251.

Ferguson, D. M., Radmer, R. J., & Kollman, P. A. (1991) *J. Med. Chem. 34*, 2654–2659.

Finzel, B. C., Poulos, T. L., & Kraut, J. (1984) *J. Biol. Chem. 259*, 13027–13036.

Frew, J. E., & Jones, P. (1984) *Adv. Inorg. Bioinorg. Mech. 3*, 175–212.

Giguere, P. A. (1950) *J. Chem. Phys. 18*, 88.

Gold, M., Wariishi, H., & Valli, K. (1989) *ACS Symp. Ser. No. 389*, 127–140.

Goodin, D. B., Mauk, A. G., & Smith, M. (1987) *J. Biol. Chem. 262*, 7719–7724.

Jones, P., & Dunford, H. B. (1977) *J. Theor. Biol. 69*, 457–470.

Mauro, J. M., Fishel, L. A., Hazzard, J. T., Meyer, T. E., Tollin, G., Cusanovich, M. A., & Kraut, J. (1988) *Biochemistry 27*, 6243–6256.

Poulos, T. L., & Finzel, B. C. (1984) *Pept. Protein Rev. 4*, 115–171.

Scheidt, W. R., Cohen, I. A., & Kastner, M. E. (1979) *Biochemistry 18*, 3546–3552.

Sivaraja, M., Goodin, D. B., Smith, M. & Hoffman, B. M. (1989) *Science 245*, 738–740.

Tien, M. (1987) *CRC Crit. Rev. Microbiol. 15*, 141–168.

Wampler, J. E., Stewart, D. E., & Gallion, S. L. (1990) In *Computer Simulation Studies in Condensed Matter Physics II* (Landau, D. P., Mon, K. K., & Schuttler, H. B., Eds., pp 68–84, Springer-Verlag, Berlin.

Weiner, P. K., & Kollman, P. A. (1981) *J. Comput. Chem. 2*, 287–303.

Weiner, S. J., Kollman, P. A., Case, D. A., Singh, U. C., Ghio, C., Alagona, G., Profeta, S., Jr., & Weiner, P. (1984) *J. Am. Chem. Soc. 106*, 765–784.

Welinder, K. G. (1985) *Eur. J. Biochem. 151*, 497–503.

Yonetani, T. (1965) *J. Biol. Chem. 240*, 4509–4514.

Yonetani, T. (1970) *Adv. Enzymol. 33*, 309.

Yonetani, T. & Ray, G. S. (1965) *J. Biol. Chem. 240*, 4503–4508.